# Detailed Pattern Computations of the UHF Antennas on the Spacecraft of the ExoMars Mission

C. Cappellin[1], E. Jørgensen[1], P. Meincke[1], O. Borries[1], C. Nardini[2], C. Dreyer[2]
[1] TICRA, Copenhagen, Denmark, cc@ticra.com
[2] Thales Alenia Space France, Cannes, France

***Abstract*—This paper describes the pattern computations of the UHF antennas mounted on the spacecraft of the EXOMARS mission. The analyses are made by the higher-order Method of Moments (MoM) add-on to GRASP and are computed twice. In the first computation, the spacecraft is modelled by perfect electrically conducting plates, properly connected by the user to each other and to the UHF antennas. This is how the problem has been solved until recently by an experienced user of GRASP. In the second computation, the detailed spacecraft geometry is imported into GRASP as a CAD file, and is automatically meshed without any requirements for the mesh connectivity.**

***Index Terms*—spacecraft, propagation.**

## I. INTRODUCTION

The ExoMars programme supported by the European and the Russian Federal Space Agencies shall characterize gas traces in the atmosphere and soil of Mars, in order to find possible biological or geological activity on the planet. Two missions are foreseen within the programme: one consisting of a Trace Gas Orbiter (TGO) plus an Entry, Descent and Landing Demonstrator Module (EDM), to be launched in 2016, and the other, featuring a rover, with launch in 2018, [1].

The TGO will carry the EDM from the Earth towards Mars, then deploy the EDM and let it land on the surface of the planet. After the landing of the EDM, the TGO will settle on a circular orbit at 400 km of altitude. From there, the instruments onboard the TGO will be deployed to accurately detect a wide range of atmospheric trace gases. With the arrival of the rover in 2018, the TGO will provide communication between the Earth and the rover located on the surface of Mars, which will drill the surface of the planet and perform a series of chemical and biological analysis.

The TGO, in the following called the spacecraft, is equipped with several antennas and instruments. Of special importance is the UHF link, provided by two UHF helix antennas. The UHF link will initially be used to monitor the EDM landing on Mars. It will then extensively be used during the second mission, to upload and send to the Earth the data collected by the rover.

The two UHF helix antennas are identical and located on a lateral side of the spacecraft. Due to their low gain and broad beam, their pattern is strongly influenced by the presence of the TGO. For a correct link, the effect of the spacecraft on the UHF antennas must therefore be known with high accuracy.

Typically [2]-[3], the evaluation of the effect of a spacecraft on the antenna pattern is a time consuming task. The antenna engineer usually models the spacecraft and the solar panels by means of a simplified model using a combination of conducting plates. To make the geometrical modelling efficient, fine details are generally disregarded, and, due to the electrical size of the spacecraft, high frequency methods are normally used. Faces which are shadowed by some parts of the spacecraft are normally not taken into account. At the low UHF frequencies, the pattern of the UHF antennas in presence of the TGO can however be computed by 3D MoM on a standard laptop, without the need for high frequency techniques. TICRA performed such a task in November 2013. The use of the 3D MoM add-on requires however a connected mesh of the full spacecraft and UHF antennas, where all faces are electrically connected to each other.

The GRASP software has recently been improved by TICRA, including several new algorithms for the detailed analysis of satellite platforms [4]. In particular, the spacecraft geometry can now be imported as a CAD file and the structure can be automatically meshed using higher-order curved quadrilaterals. The use of a recently introduced generalized integral equation implies that electrical connectivity between the faces of the spacecraft is not required [5]. The full higher-order 3D MoM allowing non-connected meshes and accelerated by a new HO-MLFMM scheme [6] is now available and will soon be released. This will save substantial time to the antenna engineer and will allow for detailed pattern computations where all fine details can be included. On the basis of the new meshing algorithm it was thus decided to repeat the UHF pattern computation and compare the results with the ones obtained in November 2013.

The purpose of the present paper is thus to describe the effect of the spacecraft on the UHF antenna pattern. This will be done twice, i.e. first in the traditional way by modelling all sides of the satellite into GRASP as electrically connected plates, and later by importing into GRASP the detailed CAD model of the spacecraft, taking advantage of the newly developed features.

The paper is organized as follows: in Section II the UHF antenna is described in detail, focusing on the modeling done in GRASP. In Section III the spacecraft is modelled by electrically connected perfectly conducting plates and its effect on the UHF antennas is shown. In Section IV the spacecraft geometry is imported into GRASP by a CAD file and the newly developed algorithms are applied. Results from Section III and Section IV are finally compared in Section V.

## II. THE UHF ANTENNA

### *A. Antenna geometry*

The UHF antenna is a quadrifilar helix antenna covered by a radome, as depicted in Fig. 1. The antenna works at 401.6 MHz and 437.1 MHz in circular polarization and was designed by Rymsa Espacio.

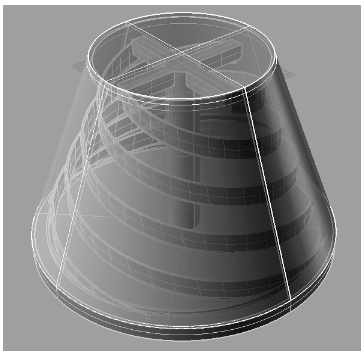

Fig. 1. The UHF quadrifilar helix antenna geometry as a CAD file.

The CAD file of the helix antenna shown in Fig. 1 was used by TICRA to derive the equation of the conical helix, and to extract the exact dimensions of the ground plane and radome of the UHF antenna. The helix was modelled in GRASP by curved wires of radius equal to 2 mm. The coordinates of the helix correspond to the mean of the helical strip seen in Fig. 1. The ground plane has a diameter of 300 mm. The thickness of the radome is 4 mm and the dielectric constant is 4.4. The final model of the UHF antenna in GRASP is shown in Fig. 2 and Fig. 3, without and with radome, respectively. It is noted that Fig. 2 and Fig. 3 show the traditional higher-order MoM mesh of the antenna used in the GRASP computations.

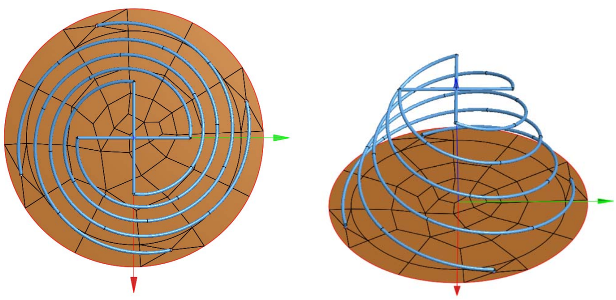

Fig. 2. GRASP model of the UHF quadrifilar helix antenna connected to the ground plane, without radome.

It is seen that all patches are electrically connected to each other and that the helixes are electrically connected to the ground plane. A red line is visible at the external edge of the circular ground plane in Fig. 2, indicating where the normal component of the current is forced to zero. No red line is visible in Fig. 3 since the radome is electrically connected to the circular ground plane, and the radome bottom face is modelled as a PEC. The antenna coordinate system is highlighted in Fig. 2 and Fig. 3: the origin is at the center of the circular ground plane, and the *x*- and *y*-axis are parallel to the arms at the top of the helixes.

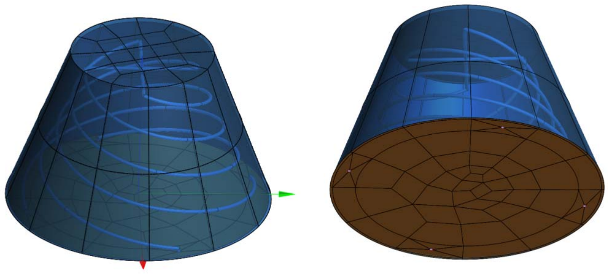

Fig. 3. GRASP model of the UHF quadrifilar helix antenna connected to the ground plane, with radome: the bottom face of the radome is pec and electrically connected to the ground plane.

### *B. GRASP pattern results*

The pattern of the UHF antenna in the antenna coordinate system was first computed without radome at *f*= 401.6 MHz and 437.1 MHz, obtaining Fig. 4. The pattern did not vary with frequency. Due to the symmetry of the antenna and the perfect circular excitation, the pattern at φ=0 deg coincides with the one at φ=45 deg and 90 deg. The cross-polar component at □=0 deg has a minimum.

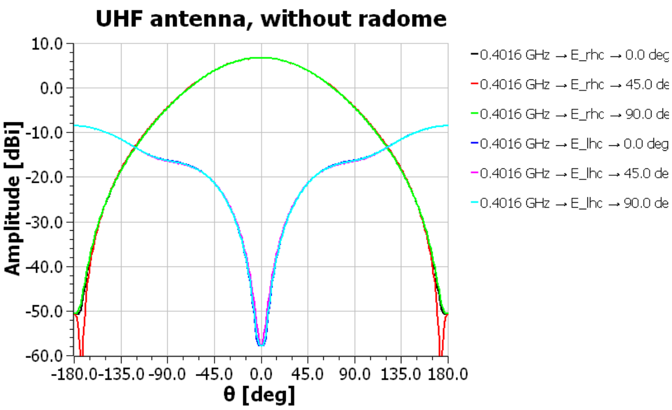


Fig. 4. GRASP pattern without radome, *f*=401.6 MHz.

Later on, the radome was added to the model, according to Fig. 3, and the new pattern was computed, see Fig. 5. Again, it could be observed that the pattern did not vary with frequency and with the phi angle. The cross-polar component at □=0 deg has still a minimum.

When the amplitude curves of Fig. 5 and Fig. 4 are compared in the same plot, it is possible to see that the presence of the radome does not produce any significant difference in the co-polar component. The cross-polar component has an increase of around 2 dB in the [±60 deg: ±180 deg] angular region, which can be considered negligible. Phase plots without and with radome showed that the phase patterns had the same shape over the entire theta domain, and were only influenced by a small shift on all phi cuts, if the radome was present. It could therefore be concluded that the radome did not influence the antenna pattern. The performances shown in Fig. 5 agreed very well with the antenna performances computed with CST by Rymsa Espacio. The helix and ground plane modelling of GRASP were therefore accurate and could be used for the remaining study.

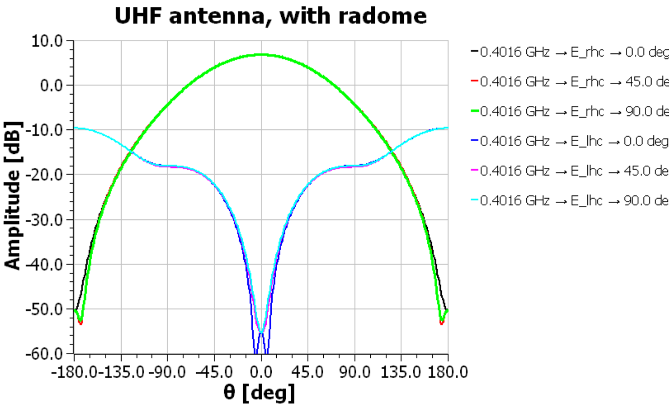


Fig. 5. GRASP pattern with radome, $f$=401.6 MHz.

## III. THE UHF ANTENNAS ON THE SPACECRAFT MODELLED BY CONDUCTING PLATES

The two UHF antennas are identical and displaced approximately by 1.3 m over a rectangular panel of 907 mm by 1748 mm. Only one antenna radiates at a time. A drawing of the panel with the two helix antennas is shown in Fig. 6. The figure shows at the same time the traditional higher-order MoM mesh that is used in the computations: the helixes are electrically connected to the panel, and all patches are electrically connected to each other. In the following we will consider the case in which the UHF A antenna radiates.

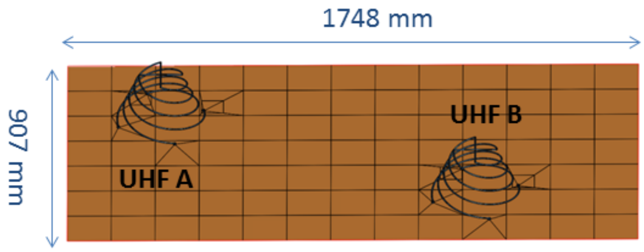


Fig. 6. Higher-order MoM mesh of the UHF A and UHF B antennas on the rectangular panel.

To model the effect of the non-radiating antenna, the four arms at the top of the helix are short circuited and the excitation is set to 0. Additional investigations have shown that this is the best way to model the effect. If the four arms are disconnected from each other modelling an open circuit, the effect of the non-radiating antenna is smaller and the pattern almost coincides with the field given by the radiating antenna, when the other antenna does not exist.

To model the spacecraft, the geometry provided by Thales was used as a starting point to produce a higher-order mesh where all satellite faces are in electrical contact with each other. The spacecraft was approximately 3.5 m by 1.75 m by 1.75 m, i.e. 4 λ by 2.3 λ by 2.3 λ. All faces and the solar panels were modelled as perfect conducting surfaces and solar panels were considered infinitely thin. The geometry of the traditional higher-order MoM mesh of the two helix antennas located on the spacecraft is shown in Fig. 13. It is noted that all patches are electrically connected everywhere, and that a red line is only visible at the external edge of the structure, as expected, indicating where the normal component of the currents is forced to zero.

The pattern of the UHF A antenna, without radome, mounted on the spacecraft and in presence of the UHF B antenna is shown in Fig. 7 for $f$=401.6 MHz. Small changes were observed at $f$=427.1 GHz. The number of patches was 1555 and the number of unknowns 10615. The matrix occupied 430 MByte. By comparing Fig. 7 with the pattern of the stand-alone UHF antenna in Fig. 4, it is seen that the influence of the spacecraft is evident, both in the co-polar and cross-polar components. The symmetry in phi disappears.

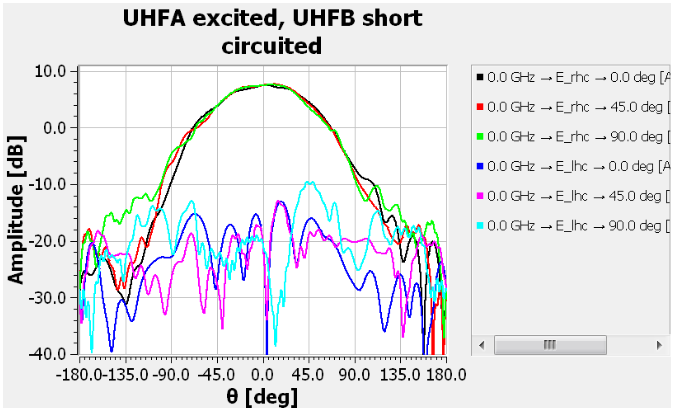


Fig. 7. GRASP pattern for the UHF A antenna in presence of the UHF B antenna on the spacecraft: without radomes and at $f$=401.6 MHz.

A plot of the total currents induced over the spacecraft can be seen in Fig. 14. It is noted that most faces of the satellites are very weakly illuminated by the UHF A antenna.

## IV. THE UHF ANTENNAS ON THE SPACECRAFT MODELLED BY CAD FILE

The CAD model of the spacecraft provided by Thales is shown in Fig. 8. Besides the two UHF antennas and the solar panels, other antennas and instruments can be seen on the spacecraft sides. The CAD file was read into the newly developed GRASP and the structure, consisting of the satellite together with the UHF antennas, was automatically meshed, without requiring electrically connected edges. The result of the mesh obtained by GRASP is shown in Fig. 15 while a zoom of the UHFA antenna on the satellite is seen in Fig. 9. There it is possible to see that the patches describing the antenna circular ground plane and the satellite side are not electrically connected, and that all fine details of the satellite are modelled. The mesh is shown in green and is transparent, meaning that the satellite body has been automatically detected as a closed PEC region. The number of patches is now 1887 and the number of unknowns is 63443, implying a MoM matrix occupying 30 GByte of memory.

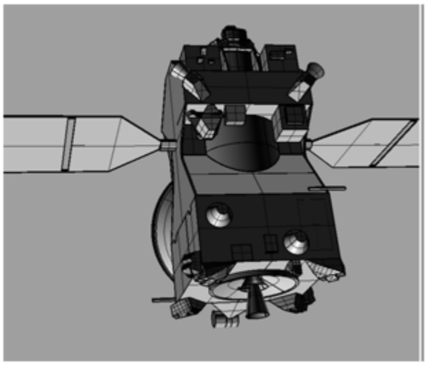

Fig. 8. CAD model of the spacecraft to be used in GRASP.

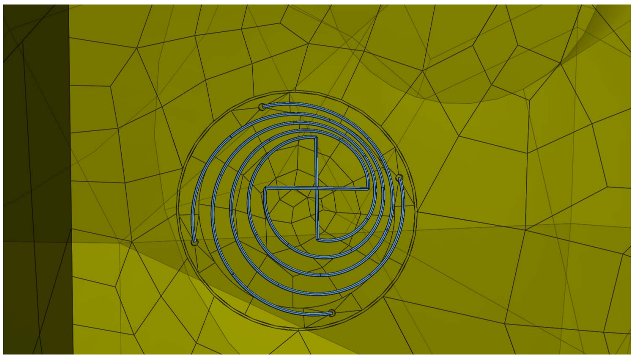

Fig. 9. Zoom of the new higher-order mesh obtained by GRASP: detail of the UHFA antenna on the satellite face.

The pattern of the UHF A antenna computed by the newly developed MoM algorithm, mounted on the spacecraft and in presence of the UHF B antenna, both without radome, is shown in Fig. 10 for *f*=401.6 MHz.

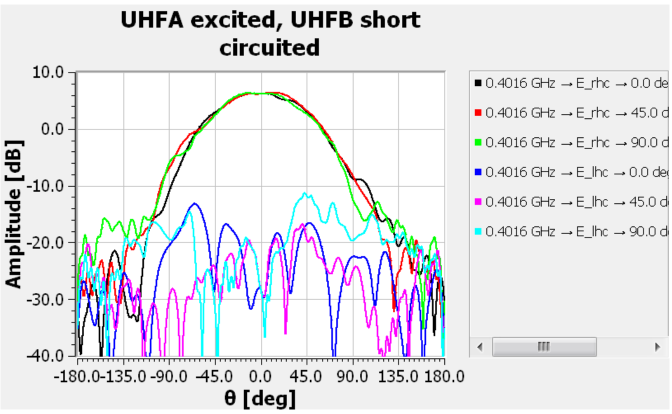


Fig. 10. GRASP pattern for the UHF A antenna in presence of the UHF B antenna on the spacecraft: without radomes and at *f*=401.6 MHz with the new MoM algorithm.

## V. COMPARISON BETWEEN THE TWO MODELLING TECHNIQUES

The pattern of Fig. 10 looks very similar to the one of Fig. 7 computed by the traditional higher-order MoM of GRASP for the simplified satellite. A comparison of the curves at $\varphi=0°$ and 90° can be seen in Fig. 11, where the results for the simplified satellite are shown by dashed lines, while the ones for the detailed satellite are continues lines. Differences in both the co-polar and cross-polar components are visible. The currents on the satellite faces are shown in Fig. 14 and Fig. 16. They both indicate that the satellite faces are weakly illuminated by the UHF antenna. Despite the low illumination, the detailed platform model has a non-negligible impact on the radiation pattern.

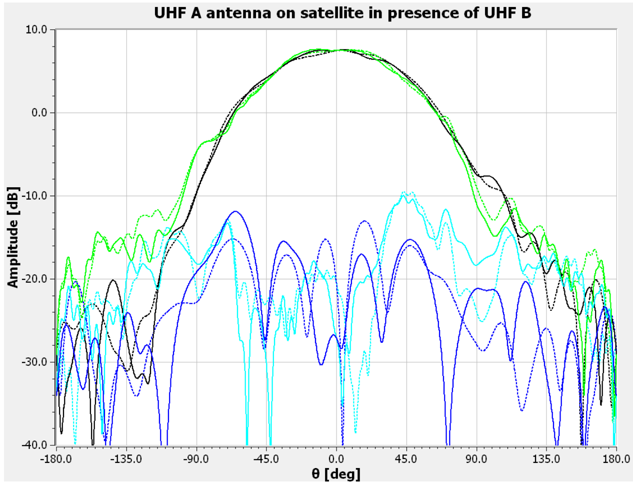


Fig. 11. Comparison of the UHF A patterns in presence of the UHF B antenna on the spacecraft: without radomes and at *f*=401.6 MHz. Continues lines are for the detailed satellite while dashed lines are for the simplified satellite model.

Finally, the two radomes were added to the UHF antennas located on the detailed satellite model and the computations were repeated. The number of patches is now 1987, i.e. 100 patches more than the ones used previously neglecting the radomes. The number of unknowns is 74779 for a very accurate higher-order MoM discretisation. Due to the relatively small electrical size the MLFMM acceleration was not used. A plot of the UHF A antenna pattern, mounted on the detailed satellite model and in presence of the UHF B antenna, with and without radomes, can be seen in Fig. 12. Dashed lines indicate results which include the presence of the radomes, while continuous lines are for results without radomes. As concluded in Section II, the radome does not play a significant role in the scattering and can be neglected.

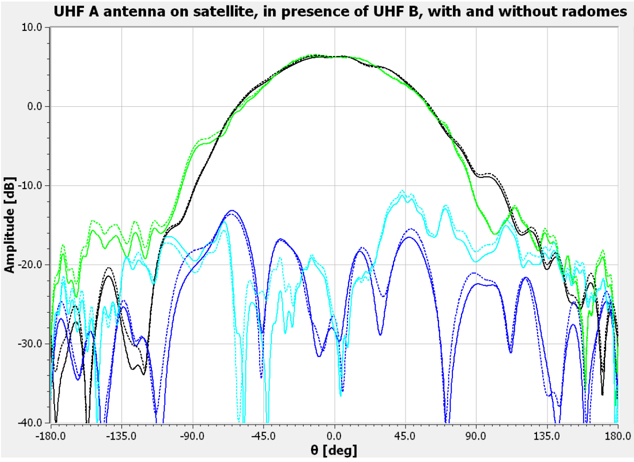


Fig. 12. GRASP pattern for the UHF A antenna in presence of the UHF B antenna on the spacecraft, at $f$=401.6 MHz with the new MoM algorithm: without radomes (continous lines) and with radomes (dashed lines).

## VI. CONCLUSIONS

The pattern computations of the UHF antennas mounted on the spacecraft of the EXOMARS mission were presented. All analyses were made by the higher-order MoM add-on to GRASP and were computed twice.

In the first computation, the spacecraft was modelled by perfect electrically conducting plates, properly connected to each other and to the UHF antennas. Building the model of the satellite with electrically connected plates was a time consuming job, which introduced some approximations: solar panels were considered infinitely thin and no additional instruments were located on the satellite faces. Moreover, the two radomes covering the UHF antennas had to be neglected since the electrical connection of the radome to the satellite faces and solar panels was a too demanding task. It was however concluded that the radome did not influence the UHF antenna pattern and thus could be neglected in the satellite scattering without introducing inaccuracies.

In the second computation, the detailed spacecraft geometry was imported into the newly developed GRASP as a CAD file, which was automatically meshed without any requirements for the mesh connectivity. It is noted that import of CAD files into GRASP usually requires pre-cleaning of the CAD model to remove electrically small features or parts defined inside closed conducting volumes. In the new detailed model, the solar panels had a finite thickness and numerous instruments and antennas were present on the satellite walls. Thanks to the algorithm which does not require electrically connected patches, an independent mesh of the radome was added to the model without the need for obtaining mesh connectivity. The inclusion of the radome confirmed the conclusion obtained earlier, namely that the radome does not influence the UHF antenna performances. Due to the detailed satellite model, more unknowns and a larger matrix were necessary in the second computation. In spite of the low illumination of the satellite faces, the inclusion of the additional details had a non-negligible impact on the patterns of the UHF antennas for wide and narrow observation angles, thus illustrating the need for detailed and accurate platform modeling.

## REFERENCES


[1] http://exploration.esa.int/mars/46124-mission-overview/

[2] F. Jensen, "Scattering from a low-orbiting satellite with rotating solar array", Proc. of 28th ESA Antenna Workshop on Space Antenna Systems and Technologies, 31 May–3 June 2005, ESTEC, Noordwijk, The Netherlands, pp. 841-844.

[3] Frank Jensen, Knud Pontoppidan, "Combining GTD with MoM in analysing the scattering from the LICEF antennas on the SMOS satellite", Proc. of European Conference on Antennas and Propagation (EuCAP 2006), Nice, France, November 6-10, 2006

[4] E. Jørgensen, O. Borries, P. Meincke, M. Zhou, N. Vesterdal, "New Fast and Robust Modelling Algorithms for Electrically Large Antennas and Platforms," submitted to EuCAP2015.

[5] Z. Peng, K.-H. Lim, and J.-F. Lee, "A discontinuous galerkin surface integral equation method for electromagnetic wave scattering from non-penetrable targets," *IEEE Trans. Antennas Propagat.*, vol. 61, no. 7, pp. 3617–3628, Jul. 2013.

[6] O. Borries, P. Meincke, E. Jørgensen, and P. C. Hansen, "Multilevel fast multipole method for higher order discretizations," *IEEE Trans. Antennas Propagat.*, vol. 62, no. 9, pp. 4695 – 4705, Sep. 2014.


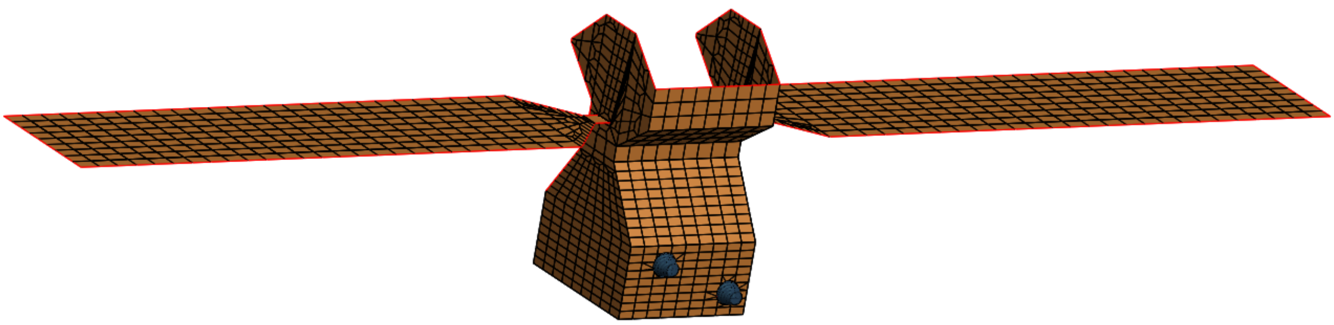

Fig. 13. Higher-order traditional MoM mesh of the spacecraft, solar panels and UHF antennas.

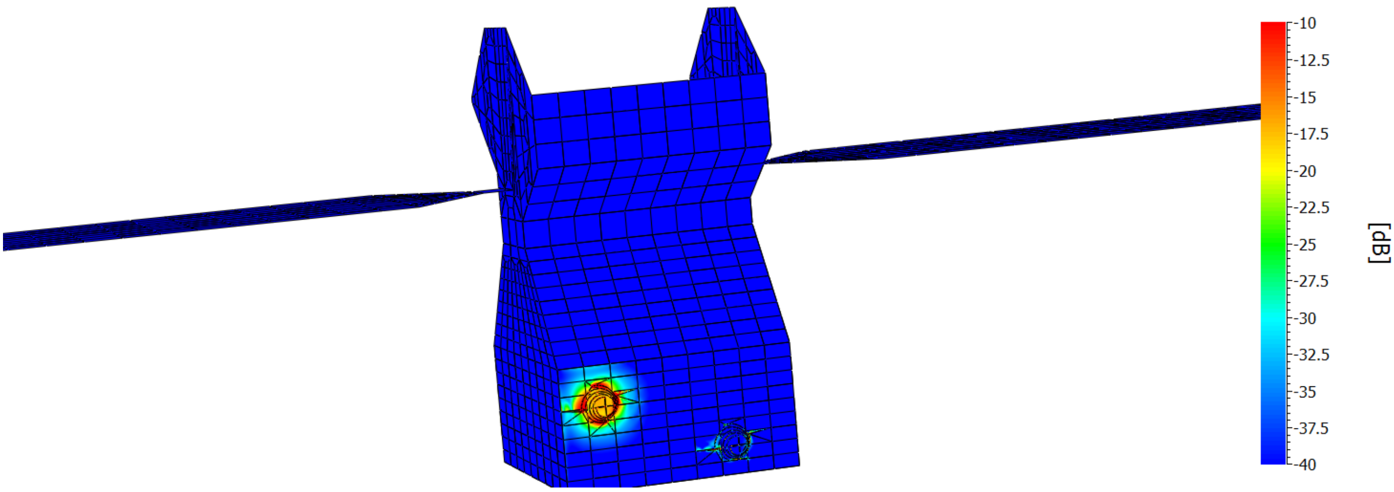


Fig. 14.  Total currents plot over the spacecraft computed with the higher-order 3D MoM of GRASP, when the UHF A antenna radiates in presence of the UHF B antenna.

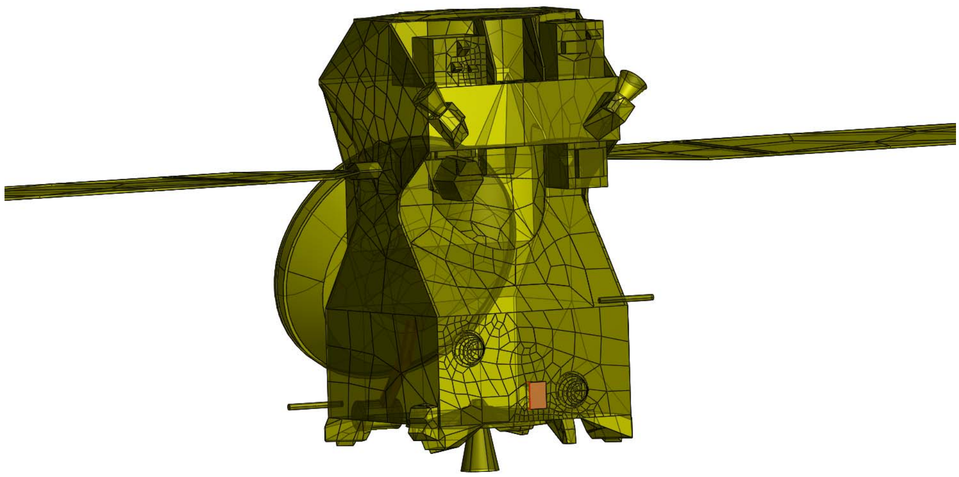

Fig. 15. Mesh of the satellite and UHF antennas, obtained by the new GRASP. The quadrilater patches are not electrically connected to each other.

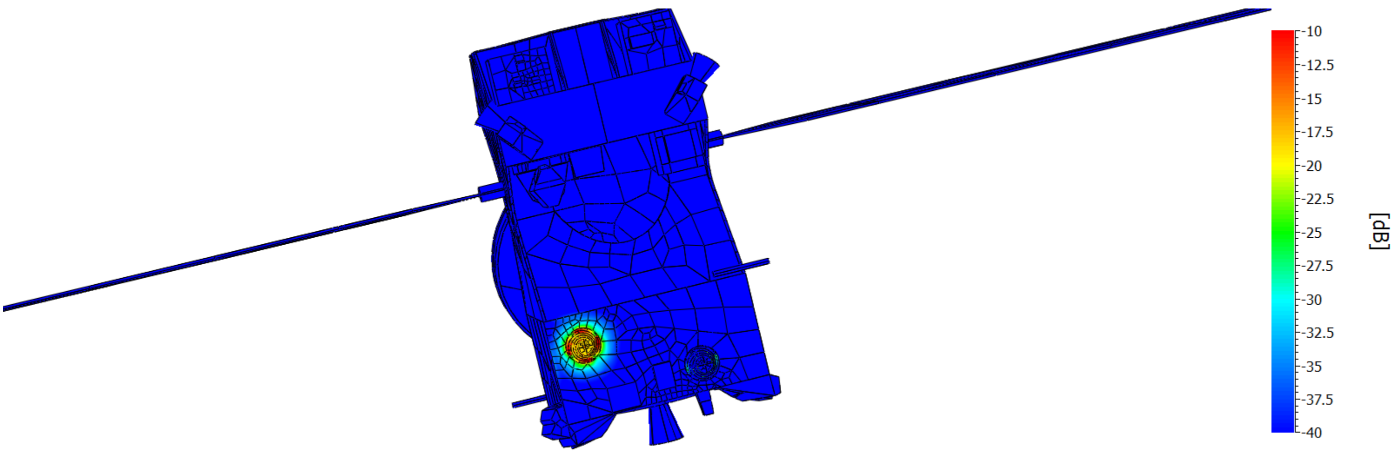


Fig. 16. Total currents plot over the spacecraft computed with the new higher-order MoM of GRASP, when the UHF A antenna radiates in presence of the UHF B antenna.